Downloaded from geology.gsapubs.org on June 24, 2010

Nanocoatings of clay and creep of the San Andreas fault at Parkfield, California

A.M. Schleicher[1], B.A. van der Pluijm[1], and L.N. Warr[2]
[1]Department of Geological Sciences, University of Michigan, 1100 North University Avenue, Ann Arbor, Michigan 48109, USA
[2]Ernst-Moritz-Arndt Universität Institut für Geographie und Geologie, F. Ludwig-Jahn-Strasse 17A, D-17487 Greifswald, Germany

ABSTRACT

Mudrock samples were investigated from two fault zones at ~3066 m and ~3296 m measured depth (MD) located outside and within the main damage zone of the San Andreas Fault Observatory at Depth (SAFOD) drillhole at Parkfield, California. All studied fault rocks show features typical of those reported across creep zones with variably spaced and interconnected networks of polished displacement surfaces coated by abundant polished films and occasional striations. Electron microscopy and X-ray diffraction study of the surfaces reveal the occurrence of neocrystallized thin film clay coatings containing illite-smectite (I-S) and chlorite-smectite (C-S) minerals. $^{40}Ar/^{39}Ar$ dating of the illitic mix-layered coatings demonstrated Miocene to Pliocene crystallization and revealed an older fault strand (8 ± 1.3 Ma) at 3066 m MD, and a probably younger fault strand (4 ± 4.9 Ma) at 3296 m MD. Today, the younger strand is the site of active creep behavior, reflecting a possible (re)activation of these clay-weakened zones. We propose that the majority of slow fault creep is controlled by the high density of thin (<100 nm thick) nanocoatings on fracture surfaces, which are sufficiently smectite-rich and interconnected at low angles to accommodate slip with minimal breakage of stronger matrix clasts. Displacements occur by frictional slip along particle surfaces and hydrated smectitic phases, in combination with intracrystalline deformation of the clay lattice, associated with extensive mineral dissolution, mass transfer, and residual precipitation of expandable layers. The localized concentration of smectite in both I-S and C-S minerals contributes to fault weakening, with fracturing and fluid infiltration creating new nucleation sites for neomineralization on displacement surfaces during continued faulting. The role of newly grown, ultrathin, hydrous clay coatings contrasts with previously proposed scenarios of reworked talc and/or serpentine phases as an explanation for weak fault and creep behavior at these depths.

INTRODUCTION

Fault creep occurs as aseismic slip in the uppermost part of the Earth's crust in the time between large stress-releasing earthquakes on active fault zones. The origin of fault creep has been the subject of intense debate (e.g., Tocher, 1960; King et al., 1973; Rosen et al., 1998), and is mostly attributed to factors including (1) low values of normal stress; (2) elevated pore-fluid pressures; and (3) low frictional strength. Along today's San Andreas fault, California, United States, several fault segments undergo creep behavior, while adjacent segments appear to show little or no creep (Rymer et al., 1984; Rosen et al., 1998). At Parkfield, active deformation of the well casing during Phase II and Phase III drilling at the San Andreas Fault Observatory at Depth (SAFOD) drillhole, together with changes in velocity, resistivity, and negligible temperature elevation at the slipping boundary at ~3.2 and 3.3 km measured depth (MD), suggest creep and characterize recent fault activity at these depths (Zoback et al., 2005; Hickman et al., 2008).

The low frictional strength of fault rock is commonly attributed to the presence of clay minerals with low frictional coefficients (Bird, 1984; Saffer et al., 2001; Morrow et al., 2007). A diverse variety of mechanically weak clay minerals has been identified within bulk rock samples recovered from the SAFOD drillhole, including illite, chlorite, illite-smectite (I-S), and chlorite-smectite (C-S) minerals (Solum et al., 2006). The occurrence of serpentine and fragments of talc has also been reported, and led to the suggestion that the formation of talc could explain the low frictional strength of this section of the San Andreas fault (Moore and Rymer, 2007; Wibberley, 2007). Localized smectitic clay mineralization has been recognized as thin film (nano) coatings on the fault rock-chip surfaces of drill cuttings and on equivalent surfaces in recovered core (Schleicher et al., 2006). These coatings are associated with polished or striated, and occasionally fibrous, fracture surfaces, features that have also been reported in other fault zones around the world (e.g., Jefferies et al., 2006; Dellisanti et al., 2008). Geochemical investigations of these mineralized SAFOD fault rocks indicate that extensive fluid-rock interaction and mass transfer occurred at these sites (Schleicher et al., 2009b), although current analyses of noble gas extracted from drilling mud indicate that the fault is currently not a site of focused fluid flow (Wiersberg and Erzinger, 2008).

In this contribution we demonstrate the specific characteristics of the secondary clay nanocoatings that neocrystallized on faults and fractures, creating a dense network of interconnected displacement surfaces along the San Andreas fault. It is proposed that dissolution-precipitation–assisted slip along microscopic smectitic phase boundaries and distributed deformation along microshear planes are plausible mechanisms to explain the creep behavior of the San Andreas fault at Parkfield and similar settings elsewhere.

GEOLOGICAL SETTING AND SAMPLES

The SAFOD drillhole is located along the creeping section of the San Andreas fault in central California (Fig. 1A). Northwest of the drillhole, the fault has a creep rate of 2.5–3.9 cm/yr (Titus et al., 2006); microearthquakes (Mw 0–2.0) are detected at shallow depths of 2–3 km (Nadeau et al., 2004). Drilling in summer 2005 successfully crossed the active trace of the San Andreas fault at ~3300 m MD with a measured temperature of ~112 °C

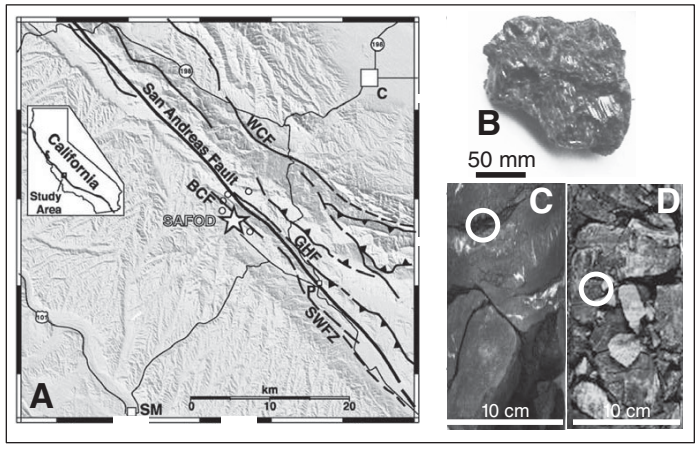

Figure 1. A: Fault map of San Andreas Fault Observatory at Depth (SAFOD) location (after Bradbury et al., 2007). BCF—Buzzard Canyon fault; WCF—Waltham Canyon fault; GHF—Gold Hill fault; SWFZ—Southwest fracture zone; P—Parkfield; SM—San Miguel; C—Coalinga. B: Typical rock chip with polished surfaces and slickensides. C, D: Fault rocks sampled from the 2005 and 2007 cores.

© 2010 Geological Society of America. For permission to copy, contact Copyright Permissions, GSA, or editing@geosociety.org.

Downloaded from geology.gsapubs.org on June 24, 2010

(Williams et al., 2005). In 2007, core material was obtained from recently active deformation zones at 3194 m and 3301 m MD (Hickman et al., 2008).

We investigated foliated fine-grained shaly fault rock samples (mudrocks) from two distinct shear zones in and outside the active creeping area of the fault at ~3066 m and ~3296 m MD (Figs. 1B–1D). The deeper sample set belongs to sedimentary rocks of the Great Valley Sequence (McDougall, *in* Bradbury et al., 2007), which separates the Cenozoic arkoses west of the San Andreas fault from the metasedimentary rocks of the Franciscan Formation to the northeast (Bradbury et al., 2007; Draper Springer et al., 2009). These fault rock specimens taken during Phase III drilling are located ~5–6 m away from the area of most intense active casing deformation (Hickman et al., 2008).

The shallow samples from the upper shear zone are situated outside the damage zone and are ~300 m above the main fault trace. These samples derive from a ~30-cm-wide, shaly, and very clay-rich shear zone positioned in the lower part of fine-grained Cenozoic arkoses containing fine-grained sandstone, siltstones, and mudstones (Solum et al., 2006; Bradbury et al., 2007; Draper Springer et al., 2009; Schleicher et al., 2009a); the zone was drilled at the end of summer 2004 (end of Phase I). Both sample sets are characterized by a scaly fabric, abundant polished fracture surfaces, and some slickensides.

ANALYTICAL METHODS

Samples were investigated using X-ray diffraction (XRD), scanning electron microscopy (SEM), and high-resolution transmission electron microscopy (HRTEM), and $^{40}Ar/^{39}Ar$ dating. The XRD and SEM-HRTEM methodology was explained in detail by Schleicher et al. (2006, 2009a). Only the $^{40}Ar/^{39}Ar$ method of fault gouge dating is outlined here (Kralik et al., 1987; van der Pluijm et al., 2001); it was used to date the timing of illite formation within clay coatings relative to the evolution of the San Andreas fault system. The effect of detrital material in the fault rock is resolved through the separation of different grain size populations, where the detrital mica component is characterized by a $2M_1$ illite polytype and the authigenic form is a 1M/1Md illite polytype. The mixture of detrital $2M_1$ polytypes and authigenic 1M/1Md is quantified by matching with WILDFIRE-calculated XRD patterns to iteratively determine the percentage of the different polytypes in several size fractions (Reynolds, 1993; Grathoff et al., 1998; Haines and van der Pluijm, 2008; Appendix DR2 in the GSA Data Repository[1]). To prevent the loss of ^{39}Ar during irradiation, the samples (~0.01 g) were packed into fused silica vials and sealed prior to irradiation (van der Pluijm et al., 2001), so that ^{39}Ar expelled from the crystallites was retained for analysis (Dong et al., 1995). The sample vials were broken open and the initial gas was analyzed prior to step-heating under a defocused laser until sample fusion occurred (Magloughlin et al., 2001).

RESULTS

Both studied sample sets contain illite and I-S minerals in the matrix, with additional chlorite and C-S in the deeper samples. Highly localized, thin precipitations of hydrous I-S and C-S mixed-layered mineral nanocoatings were also detected in both fault rocks, growing preferentially on the polished fracture surfaces, with occasional slickensides (Fig. 1B). The neocrystallized origin of these clay minerals is evident from the low-angle interlocking nature of the crystallites that lack features such as particle fragmentation or kinking that would be expected if the clay films were mechanically emplaced. A synfaulting origin for these nanocoatings of clay is also supported by the occurrence of smectitic slickenfibers reported on polished fault surfaces (Schleicher et al., 2006). Smectitic nanocoatings are of particular interest due to their specific localization and unusual physicochemical properties. Special characteristics such as ultrafine grain sizes (mean diameter of <0.2 μm), elongated particle shapes (mean aspect ratios between 1.5 and 1.9), preferred orientation produced by substrate-controlled growth, and enhanced ability to exchange cations and adsorb structured water molecules within interlayer sites are all features that contribute to weak physical strength and higher chemical reactivity (Saffer et al., 2001; Ikari et al., 2007; Morrow et al., 2007). HRTEM analyses of the separated mineral coatings show low-angle stacking arrangements of ~5–20 layers of I-S and/or C-S particles, with an average smectite lattice thickness of ~1.3–1.5 nm (Fig. 2A). Higher concentrations of smectite layers occur within ordered I-S packets (50/50 mixture) than observed in mudrock matrix I-S minerals. These minerals show deformation features, such as lattice distortion of particles and numerous layer terminations attributed to both frictional slip and dislocation creep perpendicular to c-axes. Semiquantitative chemical analysis show compositions that are typical for I-S (Fig. 2B) and C-S mixed layers (Appendix DR1), supporting the direct observations, and with the 1Md polytype nature of the authigenic mixed-layered I-S (Fig. 2C), indicates crystallization under low-temperature conditions (Inoue et al., 1987).

The $^{40}Ar/^{39}Ar$ illite ages from the SAFOD samples are shown in Figure 3 (see Appendix DR3 and Table DR1 for details). Plotting the exp (λt) – 1 age relationship (λ = decay constant, t = total gas age) as a function of the percentage detrital material, we find a lower intercept age of 4 ± 4.9 Ma for the deeper sample and 8 ± 1.3 Ma for the shallower sample. Such young ages confirm the neocrystallized origin of the I-S

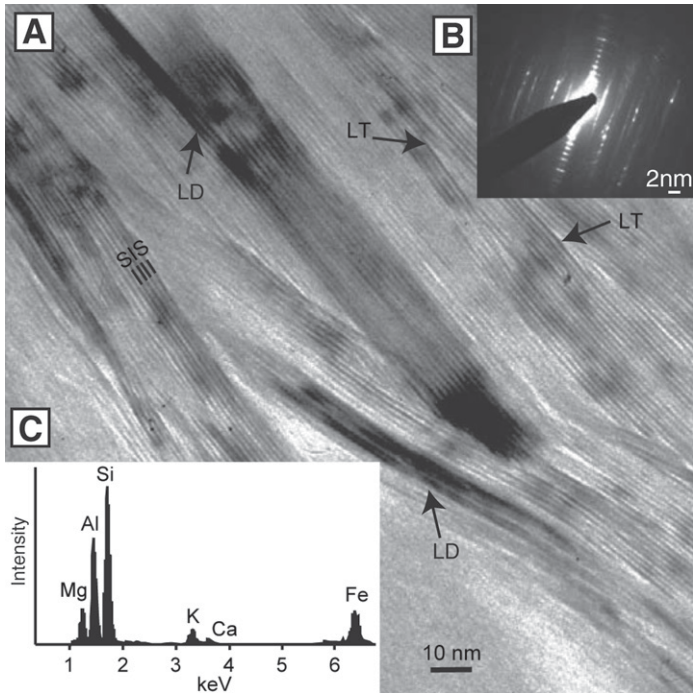

Figure 2. A: High-resolution transmission electron microscopy image of nanoclay coatings. Low-angle arrays of 5–20-nm-thick, ordered illite-smectite particles are arranged in <100-nm-thick mineralized sheets. I—Ilite; S—smectite layers; LD—lattice distortion; LT—lattice termination. B: Diffraction pattern of illite particles (1Md polytype) with streaking of nonbasal (hkl) planes. C: Chemical composition of authigenic I-S, with notable Mg and Ca in smectite interlayers.

[1]GSA Data Repository item 2010178, Appendix DR1 (TEM lattice fringe images), Appendix DR2 (best matches of calculated WILDFIRE patterns with different grain size fractions of the natural SAFOD samples at 3066 m and 3296 m measured depth), Appendix DR3 ($^{40}Ar/^{39}Ar$ spectra for different grain size fractions of fault rocks from the SAFOD drillhole at 3066 m and 3296 m), and Appendix DR4 (table of depth, grain sizes, %1M and 2M illite, total gas age and retention age data of the two sample sets), is available online at www.geosociety.org/pubs/ft2010.htm, or on request from editing@geosociety.org or Documents Secretary, GSA, P.O. Box 9140, Boulder, CO 80301, USA.

Downloaded from geology.gsapubs.org on June 24, 2010

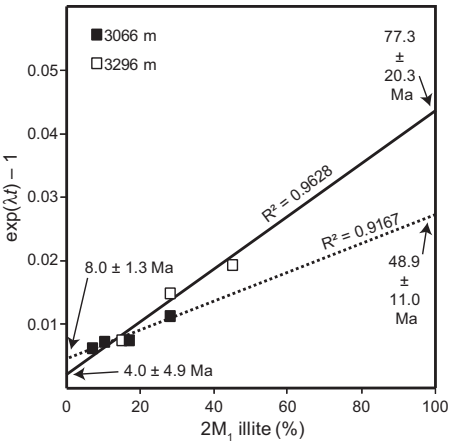

Figure 3. ^{40}Ar-^{39}Ar dating of two different shear zones. The exp (λt) – 1 age relationship of multiple size fractions for each sample is plotted against percent detrital 2M1 illite.

minerals and reflect the timing of authigenic illite formation in these two fault zones. To take into account the analytical errors involved, the fitting of the data included a York regression technique. The errors calculated for the 3296 m mudrock are relatively high due to the limited number of grain-size fractions that could be separated from this sample. However, as the error of individual analyses is typically in the range of 1–2 m.y., we consider the best fit extrapolated ages to be different enough to imply two different authigenic illite age groups for these samples. Corresponding upper intercept ages are ca. 77.3 Ma and ca. 48.9 Ma, representing the ages of detrital mica minerals in the host rocks (formation or cooling ages; see Haines and van der Pluijm, 2008). Casing deformation occurs 5–6 m below the samples investigated in the deeper fault, at ~3301 m MD, where C-S and corrensite (50/50 mixture of C-S) are the major mineral phases present on fracture coatings within foliated fault gouge. This difference in mineralogy likely reflects a change in fluid composition with time in this area, but in both sample sets the nanofilms contain significant quantities of neoprecipitated smectite layers. The upper fault at 3066 m does not currently show signs of creep activity.

DISCUSSION AND CONCLUSIONS

There is growing agreement that phyllosilicates can contribute to a mechanically weak San Andreas fault, but there are contrasting opinions as to which, if any, minerals are responsible for this behavior along the creeping section sampled by the SAFOD drillhole. Wu et al. (1975) proposed the importance of hydrated clays like smectite in the San Andreas fault from experimental observations, whereas Moore and Rymer (2007) and Wibberley (2007) emphasized that talc provides the mechanical connection between serpentinite and creep in the San Andreas fault. However, our observations do not find an adequate presence of talc in these rocks. Instead, we report neocrystallized, hydrous mixed-layered clay minerals, namely I-S and C-S, forming thin films (to 100 nm thick), which we interpret grew on fracture surfaces during fault creep. These hydrated clays have frictional properties comparable to those of talc at ~3 km depths, with increasing water content lowering the frictional strength (Morrow et al., 2007). Although we can only speculate on the nature of these mixed-layered clays at depths beyond that of the SAFOD drilling, comparisons with other hydrothermal and low-temperature metamorphic environments, where such phases precipitate up to ~250 °C, suggests that these phases could be present at significantly greater crustal depths (Merriman and Peacor, 1999). Under such conditions, the thermodynamic calculations of Bird (1984) predict that a Ca-smectite phase would still maintain a 1-water structure (containing ~10% H_2O) within its interlayer. Assuming a normal continental geothermal gradient, such a hydrated structure would be stable down to ~10 km depth, at a lithostatic pressure of ~250 MPa and a temperature of ~250 °C.

We consider the localization of the smectitic thin film coatings to be a key feature to explain slow creep along fracture surfaces. During active fault movement the low permeability of the coated surfaces can build up very small scale and localized fluid pressures, as the water cannot quickly escape from the smectite interlayers and associated clay-coated pores. We conclude that the I-S and C-S minerals first formed during Miocene to Pliocene time (ca. 4–8 Ma), when the respective strands of the San Andreas fault system were deforming, producing fracture surfaces that allowed dissolution-precipitation and the deposition of surface coating from circulating fluids. Once a sufficient network of surface coating was established, and the concentration and interconnection of the low-permeability clay-sealed fractures reached a certain threshold, the fault zone could deform by creep, as is today observed near the deeper fault strand.

Based on our observations, we propose a model for the evolution of fault rocks and the role of nanocoatings in creating a mechanically weak upper part of the San Andreas fault, shown in the schematic diagram of Figure 4. Following initial fracture generation during (microseismic) displacement, nucleation and mineralization processes occur on fracture surfaces where reactive fluids are able to circulate along these rock interfaces and deposit hydrated clay phases. The formation of I-S versus C-S is dependent on the chemical activity of K^+- and Mg^{2+}-rich fluids (Offler and Prendergast, 1985), sourced by remote or local dissolution of K-feldspars, white mica, and a range of mafic minerals present in the host rocks. The importance of fluids is further illustrated by the abundance of the mineralized veins in most of the surrounding rocks (Kirschner et al., 2005; Mittempergher et al., 2009). Mineral dissolution and neomineralization of smectite phases along active faults and fractures are processes that probably continue during creep and fault reactivation, until a seismic event abandons the weak strand and produces higher concentrations of clay-coated fracture surfaces in a nearby area. This type of reaction weakening is, however, only expected to lead to creep when the weak nanocoated fractures are distributed and well connected and are at low angles to the direction of slip, a condition we suggest is fulfilled in the currently active creep zones characterized by fault rocks with intense scaly fabrics. Based on these inferences and our observations of young, ultrathin, hydrated clay coatings on recovered displacement surfaces in the Parkfield section of the San Andreas fault, we conclude that the localization of clay minerals on contact surfaces promotes today's creep behavior, rather than occasional matrix minerals (such as talc) that do not otherwise show a strong genetic link to recent faulting. These controls have operated at least over the past ~4–8 m.y. of fault activity.

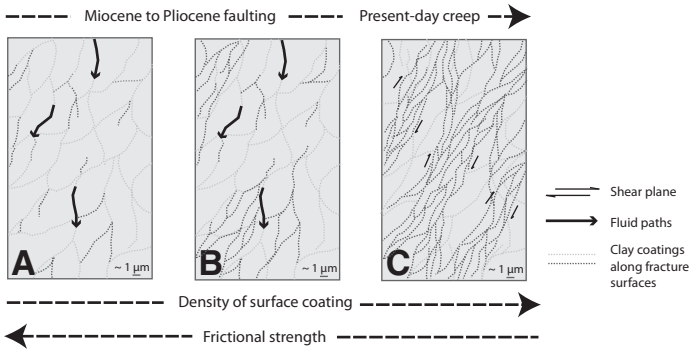

Figure 4. Schematic illustration of evolution of fault rocks and development and role of nanocoatings in mechanically weak San Andreas fault. A: Initial fracture generation during (microseismic) displacement is followed by fluid circulation and (B) nucleation, dissolution, and mineralization processes on fracture surfaces with deposition of hydrated clay phases. C: Creep is then located along the interconnected nano-coated fractures within mudrock fractured shale horizons.

Downloaded from geology.gsapubs.org on June 24, 2010

ACKNOWLEDGMENTS

Our research was supported by National Science Foundation grants EAR-0345985 and EAR-0738435 (van der Pluijm) and Deutsche Forschungsgemeinschaft grant SCHL 1821/1-1 and 1821/1-2 (Schleicher). We thank Carl Henderson and Chris Hall at the University of Michigan for support with microscopy analyses and Ar chronology, and the San Andreas Fault Observatory at Depth (SAFOD) science team for sampling and support, both onsite and offsite. We thank R.E. Holdsworth and two anonymous reviewers for their helpful comments, which greatly improved the manuscript.

REFERENCES CITED

Bird, P., 1984, Hydration-phase diagrams and friction of montmorillonite under laboratory and geologic conditions, with implications for shale compaction, slope stability, and strength of fault gouge: Tectonophysics, v. 107, p. 235–260, doi: 10.1016/0040-1951(84)90253-1.

Bradbury, K.K., Barton, D.C., Solum, J.G., Draper, S.D., and Evans, J.P., 2007, Mineralogic and textural analyses of drill cuttings from the San Andreas Fault Observatory at Depth (SAFOD) boreholes: Initial interpretations of fault zone composition and constraints on geologic models: Geosphere, v. 5, p. 299–318, doi: 10.1130/GES00076.1.

Dellisanti, F., Pini, G.A., Tateo, F., and Baudin, F., 2008, The role of tectonic shear strain on the illitization mechanism of mixed-layers illite-smectite. A case study from a fault zone in the Northern Apennines, Italy: International Journal of Earth Sciences, v. 97, p. 601–616, doi: 10.1007/s00531-007-0180-4.

Dong, H., Hall, C., Peacor, D., and Halliday, A., 1995, Mechanism of argon retention in clays revealed by laser Ar-Ar dating: Science, v. 267, p. 355–359, doi: 10.1126/science.267.5196.355.

Draper Springer, S., Evans, J.P., Garver, J.I., Kirschner, D., and Janecke, S.U., 2009, Arkosic rocks from the San Andreas Fault Observatory at Depth (SAFOD) borehole, central California: Implications for the structure and tectonics of the San Andreas fault zone: Lithosphere, v. 1, p. 206–226, doi: 10.1130/L13.1.

Grathoff, G., Moore, D., Hay, R., and Wemmer, K., 1998, Illite polytype quantification in Paleozoic shales: A technique to quantify diagenetic and detrital illite, *in* Schieber J., et al., eds., Shale and mudstones II. Petrography, petrophysics, geochemistry, and economic geology: Stuttgart, Germany, Schweizerbartsche Verlagsbuchhandlung, p. 161–175.

Haines, S.H., and van der Pluijm, B.A., 2008, Clay quantification and Ar-Ar dating of synthetic and natural gouge: Application to the Miocene Sierra Mazatan detachment fault, Sonora, Mexico: Journal of Structural Geology, v. 30, p. 525–538, doi: 10.1016/j.jsg.2007.11.012.

Hickman, S., Zoback, M., Ellsworth, W., Chester, J., Chester, F., Evans, J., Moore, D., Kirschner, D., Schleicher, A., van der Pluijm, B., and Solum, J., 2008, Structure and composition of the San Andreas fault in central California: Recent results from SAFOD sample analyses: Eos (Transactions, American Geophysical Union), v. 89, Fall meeting supplement, abs. T 53F–01.

Ikari, M.J., Saffer, D.M., and Marone, C., 2007, Effect of hydration state on the frictional properties of montmorillonite-based fault gouge: Journal of Geophysical Research, v. 112, B06423, doi: 10.1029/2006JB004748.

Inoue, A., Velde, B., Meunier, A., and Touchard, G., 1987, Mechanism of illite formation during smectite-to-illite conversion in a hydrothermal system: American Mineralogist, v. 73, p. 1325–1334.

Jefferies, S.P., Holdsworth, R.E., Wibberly, C.A.J., Shimamoto, T., Spiers, C.J., Niemeijer, A.R., and Lloyd, G.E., 2006, The nature and importance of phyllonite development in crustal-scale fault cores: An example from the Median Tectonic Line, Japan: Journal of Structural Geology, v. 28, p. 220–235, doi: 10.1016/j.jsg.2005.10.008.

King, C.Y., Nason, R.D., and Tocher, D., 1973, Kinematics of fault creep: Royal Society of London Philosophical Transactions, ser. A, v. 274, p. 355–360, doi: 10.1098/rsta.1973.0063.

Kirschner, D.L., Evans, J., Chester, J., Chester, F., Solum, J., and Moore, D., 2005, Elemental and stable isotope chemistry of cuttings and core samples from SAFOD drill hole: Eos (Transactions, American Geophysical Union), v. 86, abs. T21A-0452.

Kralik, M., Klima, L., and Riedmueller, G., 1987, Dating fault gouges: Nature, v. 327, p. 315–317, doi: 10.1038/327315a0.

Magloughlin, J.F., Hall, C.M., and van der Pluijm, B.A., 2001, Ar-Ar geochronometry of pseudotachylites by vacuum encapsulation: North Cascade Mountains, Washington, USA: Geology, v. 29, p. 51–54, doi: 10.1130/0091-7613(2001)029<0051:AAGOPB>2.0.CO;2.

Merriman, R.J., and Peacor, D.R., 1999, Very low grade metapelites: Mineralogy, microfabric and measuring reaction progress, *in* Frey, M., and Robinson, D., eds., Low-grade metamorphism: Oxford, UK, Blackwell Science, p. 10–58.

Mittempergher, S., Di Toro, G., Gratier, J., Hadizadeh, J., Smith, S.A., Desbois, G., and Spiess, R., 2009, Evidences of transient increase of fluid pressure in isolated patches of the active San Andreas Fault in SAFOD phase III cores: Eos (Transactions, American Geophysical Union), v. 90, abs. T52B–04.

Moore, D.E., and Rymer, M.J., 2007, Talc bearing serpentinite and the creeping section of the San Andreas fault: Nature, v. 448, p. 795–797, doi: 10.1038/nature06064.

Morrow, C., Solum, J., Tembe, S., Lockner, D., and Wong, T.F., 2007, Using drill cutting separates to estimate the strength of narrow shear zones at SAFOD: Geophysical Research Letters, v. 34, L11301, doi: 10.1029/2007GL029665.

Nadeau, R.M., Michelini, A., Uhrhammer, R.A., Dolenc, D., and McEvilly, T.V., 2004, Detailed kinematics, structure, and recurrence of microseismicity in the SAFOD target region: Geophysical Research Letters, v. 31, doi: 10.1029/2003GL019409.

Offler, R., and Prendergast, E., 1985, Significance of illite crystallinity and b0 values of K-white mica in low-grade metamorphic rocks, North Hill End synclinorium, New South Wales, Australia: Mining Magazine, v. 49, p. 357–364.

Reynolds, R., Jr., 1993, WILDFIRE: A computer program for the calculation of three-dimensional powder X-ray diffraction patterns for mica polytypes and their disordered variations: Hanover, New Hampshire, R.C. Reynolds.

Rosen, P., Werner, C., Fielding, E., Hensley, S., Buckley, S., and Vincent, P., 1998, Aseismic creep along the San Andreas Fault northwest of Parkfield, CA measured by radar interferometry: Geophysical Research Letters, v. 25, p. 825–828 doi: 10.1029/98GL50495.

Rymer, M.J., Lisowski, M., and Burford, R.O., 1984, Structural explanation for low creep rates on the San Andreas fault near Monarch Peak, central California: Seismological Society of America Bulletin, v. 74, p. 925–931.

Saffer, D.M., Frye, K., Marone, C., and Mair, K., 2001, Laboratory results indicating weak and potentially unstable frictional behavior of smectite clay: Geophysical Research Letters, v. 28, p. 2297–2300, doi: 10.1029/2001GL012869.

Schleicher, A.M., van der Pluijm, B.A., and Warr, L.N., 2006, Origin and significance of clay-coated fractures in mudrock fragments of the SAFOD borehole (Parkfield, California): Geophysical Research Letters, v. 33, L16313, doi: 10.1029/2006GL026505.

Schleicher, A.M., Warr, L.N., and van der Pluijm, B.A., 2009a, On the origin of mixed-layered clay minerals from the San Andreas fault at 2.5–3 km vertical depth (SAFOD drillhole at Parkfield, California): Contributions to Mineralogy and Petrology, v. 157, p. 173–187, doi: 10.1007/s00410-008-0328-7.

Schleicher, A.M., Tourscher, S., van der Pluijm, B.A., and Warr, L.N., 2009b, Constraints on mineralization, fluid-rock interaction and mass transfer during faulting at 2–3 km depth from the SAFOD drill hole: Journal of Geophysical Research, v. 114, B04202, doi: 10.1029/2008JB006092.

Solum, J.G., Hickman, S.H., Lockner, D.A., Moore, D.E., van der Pluijm, B.A., Schleicher, A.M., and Evans, J.P., 2006, Mineralogical characterization of protolith and fault rocks from the SAFOD Main Hole: Geophysical Research Letters, v. 33, L21314, doi: 10.1029/2006GL027285.

Titus, S.J., DeMets, C., and Tikoff, B., 2006, Thirty-five-year creep rates for the creeping segment of the San Andreas fault and the effects of the 2004 Parkfield earthquake: Constraints from alignment arrays, continuous global positioning system, and creepmeter: Seismological Society of America Bulletin, v. 96, p. S250–S268, doi: 10.1785/0120050811.

Tocher, D., 1960, Creep on the San Andreas fault—Creep rate and related measurements at Vineyard, California: Seismological Society of America Bulletin, v. 50, p. 396–404.

van der Pluijm, B.A., Hall, C., Vrolijk, P., Pevear, D., and Covey, M., 2001, The dating of shallow faults in the Earth's crust: Nature, v. 412, p. 172–175, doi: 10.1038/35084053.

Wibberley, C., 2007, Talc at fault: Nature, v. 448, p. 756–757, doi: 10.1038/448756a.

Wiersberg, T., and Erzinger, J., 2008, Origin and spatial distribution of gas at seismogenic depths of the San Andreas fault from drill-mud gas analysis: Applied Geochemistry, v. 23, p. 1675–1690, doi: 10.1016/j.apgeochem.2008.01.012.

Williams, C.F., d'Alessio, M.A., Grubb, F.V., and Galanis, S.P., Jr., 2005, Heat flow studies in the SAFOD main hole: Eos (Transactions, American Geophysical Union), v. 86, abs.T23E-07.

Wu, F.T., Blatter, L., and Roberson, H., 1975, Clay gouges in the San Andreas fault system and their possible implications: Pure and Applied Geophysics, v. 133, p. 87–95, doi: 10.1007/BF01592901.

Zoback, M., Hickman, S., and Ellsworth, W., 2005, Drilling, sampling and measurements in the San Andreas fault zone at seismogenic depth: Eos (Transactions, American Geophysical Union), v. 87, Fall meeting supplement, abs. T23E–01.

Manuscript received 2 February 2010
Revised manuscript received 11 February 2010
Manuscript accepted 26 February 2010

Printed in USA